Arabian Journal of Chemistry (2023) **16**, 105135

King Saud University

Arabian Journal of Chemistry

www.ksu.edu.sa
www.sciencedirect.com

ORIGINAL ARTICLE

Stabilization of zirconia nanoparticles by collagen protein and calcium carbonate extracted from eggshell and its biodegradation, radical scavenging and mineralization activity

Summeya Akram [a], Mahwish Bashir [a,*], Farzana Majid [b], Maida Ayub [a], Babar Shahzad Khan [a], Adnan Saeed [a], Mohammed Rafi Shaik [c], Mujeeb Khan [c], Baji Shaik [d]

[a] *Department of Physics, Govt. College Women University, Sialkot, Pakistan*
[b] *Department of Physics, University of the Punjab, Lahore, Pakistan*
[c] *Department of Chemistry, College of Science, King Saud University, P.O. Box 2455, Riyadh 11451, Saudi Arabia*
[d] *School of Chemical Engineering, Yeungnam University, Gyeongsan 38541, Republic of Korea*

Received 9 February 2023; accepted 3 July 2023
Available online 6 July 2023

KEYWORDS

Eggshell;
ZrO_2;
Tetragonal;
Biodegradation;
Antioxidant;
Bone implantation

Abstract In this current study, collagen protein extracted from eggshell membrane and calcium carbonate (a main component of eggshell) are used as additive to enhance the stability and hardness of the zirconia crystals. Five different samples are prepared by adding membrane containing eggshell content as, 1 g, 2 g, 3 g, 4 g and 5 g in aqueous zirconium oxychloride sol. Phase purity is confirmed by XRD and FTIR. Phase pure and dense particles divulges the high hardness (~1389 HV) and fracture toughness (12.89 MPa $m^{1/2}$). FESEM analysis illustrates the formation of dense, well separated, non-agglomerated and spherical nanoparticles at 5 g of eggshell content. Eggshell works as a surfactant and stabilizer for formation of phase pure tetragonal spherical nanoparticles. Biodegradation study of optimized tetragonal zirconia (t-ZrO_2)in phosphate buffered saline (PBS) presents that minor change in weight and hardness after 72 h of immersion. Antioxidant study shows the 96% of radical scavenging activity (RSA). In vitro bio-mineralization study shows the formation of new bone after 5 weeks. After 5 weeks all pores were filled and minerals were deposited on the surface of the scaffolds. SEM images confirms that eggshell-zirconia composite form new bone. So eggshell addition results in formation of phase pure t-ZrO_2 nanoparticles with

* Corresponding author.
E-mail address: mahwish.bashir@gcwus.edu.pk (M. Bashir).
Peer review under responsibility of King Saud University.

Production and hosting by Elsevier

https://doi.org/10.1016/j.arabjc.2023.105135

well-defined boundaries which exhibit higher hardness, fracture toughness, stability and enhanced antioxidant properties.

1. Introduction

Oxides present outstanding structural, mechanical and biocompatible properties (Shadianlou et al., 2022; Bapat et al., 2022). Zirconium oxide/zirconia is widely studied oxide for biological applications. Apart from its exceptional mechanical qualities, zirconia also possesses beneficial biological characteristics such as low corrosion potential, lower toxicity, as well as little bacterial adherence. Although since 1970s, a vast amount of biomedical research has focused on ways to employ zirconia in medicine and dentistry, notably in stress-bearing positions in which its strength equals that of several alloys (Chen and Moussi, 2016). But main problem arises related to zirconia is its stability and density. Monoclinic (m), cubic (c), as well as tetragonal (t) crystalline phases of zirconia significantly depend on ambient temperature (Limbu, 2022). In monoclinic geometry, which is found in natural deposits, is the most durable at normal temperature under standard pressure. At 1170 °C, the monoclinic phase transforms into a tetragonal phase, with a 4–5% volume shrinking. At 2370 °C, the tetragonal phase shrinks even further plus becomes cubic (Cho et al., 2023).

Zirconia's biomedical applications, mechanical strength, as well as low corrosion potential has made it a popular choice for dentistry filling and bone implantations, especially when aesthetics are important. Through use of zirconia in dentistry was originally mentioned in the 1970s (Cranin and Schnitman, 1975). In 2008, zirconia is being used for the first time as just an endosseous dental implant (Hoffmann et al., 2008).

For the production of ZrO_2, literature investigations reveal two major synthesis techniques. (a) Traditional sol–gel procedures (Bagbi et al., 2016) and (b) precipitation techniques (Fedorenko et al., 2022). Because the characteristics of nanostructures might change from 3D to 2D or 1D, an appropriate synthesizing process is crucial for characterizing them (Mahmood and Afzal, 2013). Chemical solution-based approaches offer a vast range of additives to be incorporated into the host to improve structural as well as mechanical properties. The endurance as well as interaction with organic compounds found in body fluids, including such, is critical. In current study, eggshell is added into zirconia as egg-shell is a bio-ceramic produced at ambient temperature and having fastest calcifying process. Chicken eggshell composed of 6 g of mineral. Mainly, chicken eggshell composed of 96% of $CaCO_3$, 2% of organic matrix, Mg, P and some traces of other elements (Hincke et al., 2012). Specific composition of chicken eggshell is given in Table 1. Eggshell membrane (ESM) contain a fibrous protein known as collagen confirms that organic matrix derived from (ESM) is not rigid. It is expected that when ESM is added in nanomaterial results in macro pores (Tsai et al., 2006). The main role of ESM protein is to form new bone and cartilage formation that assist molecules to bond with body (Rasheed et al., 2019). A zirconia scaffold can integrate collagen to add mechanical support without impacting other qualities. Within six months of surgery, Katsube et al. (Katsube et al., 2000) discovered that the locations repaired with chondrocytes grown in collagen gel had superior histology scores. Kaizawa et al. (Kaizawa et al., 2019) isolated collagen from human tendons and processed it into hydrogels. The findings demonstrated that, in comparison to the control group, collagen helps to repair the bones. Hydrogels made of chitosan and collagen have also been shown biocompatibility, aid in bone conduction, and encourage bone growth. Alginate/collagen gels were created by Jin et al. (Jin and Kim, 2018) to maintain the cartilage phenotype and stop cartilage differentiation. The findings demonstrated that cells multiplied over time in all gels, with the composite gel exhibiting the highest levels of proliferation. Using an in situ mineralization approach, Takallu et al. (Takallu et al., 2019) produced dense hydroxyapatite (HA) particles in collagen solution. The findings showed that HA particles filled in the gaps in the collagen network and, through their interactions, raised the crosslinking density of the scaffolds, decreasing their ability to swell. Additionally, HA microspheres with a finer structure have advanced quickly. Collagen/chitosan composite scaffolds were created by Kafi et al. (Kafi et al., 2019) to boost hMSC adhesion and proliferation while enhancing mechanical strength. In literature, different additives have used for synthesis of stabilized zirconia but relatively high temperatures (Bashir et al., 2018; Okada et al., 2019). It is worth mentioning here, eggshell is first time used to stabilize zirconia. Parera (Parera, 1992) reported that zirconia catalyst was prepared by using $ZrClO_2$ salt. This prepared ZrO_2 was heated at various temperatures. Pure t-ZrO_2 was obtained at 893 K. Sohen at el. (Son et al., 2001) depicted that zirconium sulfate to synthesize zirconia. t-ZrO_2 remained stabilized at calcination temperature of 500 °C. In literature, t-ZrO_2 stability was obtained at temperature > 500 °C (Siddiqui et al., 2012). You et al. (You et al., 2012) delineated the synthesis of ultrathin films using $ZrCl_4$ by sol gel method with dispersion of zirconium halide in 1-octanol solvent. Amorphous structure was obtained after calcination at 600 °C. Bhowmick et al. (Bhowmick et al., 2017) reported chitosan, polyethylene glycol and hydroxyapatite added zirconia macropores for bone implantations. They concluded that addition of organic additives enhances the mechanical strength, antimicrobial property and cytocompatibility of zirconia. Bagbi et al. (Bagbi et al., 2016) reported the spherical gelatin A added zirconia nanoparticles and obtained monoclinic phase with crystallite size ~10.3 nm.

Here, different eggshell content is utilized to stabilize t-ZrO_2 . The goal of this research is to achieve novel zirconia for dentistry and bone implantation purpose. Effect of eggshell content on zirconia structural, morphological, mechanical antioxidant biodegradation and mineralization of hydroxyapatite is studied. It is worth mentioning here that for eggshell is used as additive for stabilization of t-ZrO_2. Eggshell with membrane will provide two major components of bone Ca and collagen which play main role for new bone and cartilage formation.

Table 1 Chemical composition of chicken eggshell.

Chemical	Chemical composition (wt%)
CaO**	96.87
MgO	0.77
SO_3	0.53
RuO	0.53
SiO_2	0.39
K_2O	0.22

** After heating $CaCO_3$ converted into CaO and CO_2.

2. Experimental details

2.1. 1 Materials and methods

Zirconium oxychloride octa-hydrate, $ZrOCl_2{\cdot}8H_2O$ (Sigma Aldrich) and de-ionized (DI) water were used as starting material. Eggshells with membrane were used as organic additive.

2.1.1. Eggshell powder

White chicken eggshells with membrane were dried in oven at 50 °C. Dried shells were grinded and powdered. Eggshells were used as additive because they mainly consists of calcium composites which are essential component for bones. Along with calcium membrane contains protein (collagen) which helps to absorb calcium in the body.

2.1.2. Synthesis of zirconia

32.25 g of $ZrOCl_2{\cdot}8H_2O$ was dissolved in 500 ml DI and stirred at room temperature. When $ZrOCl_2{\cdot}8H_2O$ reacts with DI water, hydrochloric acid and Zr $(OH)_4$ are produced [Eq. (1)]. As HCl have high boiling temperature so it evaporates. Its boiling temperature is about −85.05 °C which makes it volatile at room temperature. It is earlier reported before formation of tetragonal ZrO_2, $Zr(OH)_4$ forms, an amorphous phase called metastable phase (Tyagi et al., 2006; Zientara et al., 2013). In sol–gel process, pH, molarity and choice of precursor play an important rule for phase stabilization. Molarity of the sol was optimized earlier (Riaz et al., 2015) for formation of stabilized zirconia. $ZrOCl_2{\cdot}8H_2O$ contains 2 oxy-bridges which prefer fabrication of ZrO_2.

$$ZrOCl_2.8H_2O + 2H_2O \rightarrow Zr(OH)_4 + 7H_2O + 2HCl \quad (1)$$

1, 2, 3 4, and 5 g of eggshell powder was added per 100 ml sol. During synthesis of zirconia nanoparticles eggshells attached with zirconium. When organics are present over the surface of particles the chance of hydrostatic strains is lesser. They may coat the surface of particles and repelled water molecules. Adsorption or absorption of water molecules mainly cause the transformation of tetragonal zirconia to monoclinic zirconia or instability in phase purity. Presence of OH water molecules results in slightly larger volume. These nanoparticles were synthesized without any further heating. As high temperature lack or absence of eggshell coating to zirconia results in absorption of water, which leads to filling of oxygen vacancies explain by Kroger–Vink equation [Eq. (2)] can be written for the reaction between water and zirconia (Redfern et al., 2001). This occupancy of oxygen vacancy states leads to higher content of monoclinic zirconia (Chevalier et al., 2009). This mechanism is explained by Chevlier's model [Fig. 1].

$$H_2O + V_0^{\cdot} + O_0^x \overset{ZrO_2}{\leftrightarrow} 2OH_O \quad (2)$$

The above mixtures were stirred at room temperature. Meanwhile, 2 M of NaOH was added dropwise to obtain pH 9. pH of the starting sol for formation of t-ZrO_2 is optimized earlier (Sanaullah et al., 2021). At various pH levels, Denkewicz et al. model's (Denkewicz et al., 1990) to generate crystalline zirconia. It claims that Zr^+ and OH^- ions play a major role in controlling zirconia's crystallization. t-ZrO_2 is usually produced when was designed OH^- ions are present in higher concentrations. Mineralizer additions, such as NaOH and NH_3, are crucial for determining phase content and particle size. The crystallization process can be used to understand the impact of the mineralizer and pH. Nucleation and grain development are the two main stages of the crystallization process. Tetramer complex $[Zr_4(OH)_8(H_2O)_{16}]^{8+}$ is created when $ZrOCl_2{\cdot}8H_2O$ is combined with DI water [Eq. (3)]. This tetramer comprises of 16 nearby water molecules and 8 hydroxo bridges (OH) (Firth et al., 2021). A specific amount of H^+ ions from the nearby water would be released when the pH of the sol changes to basic tetramer.

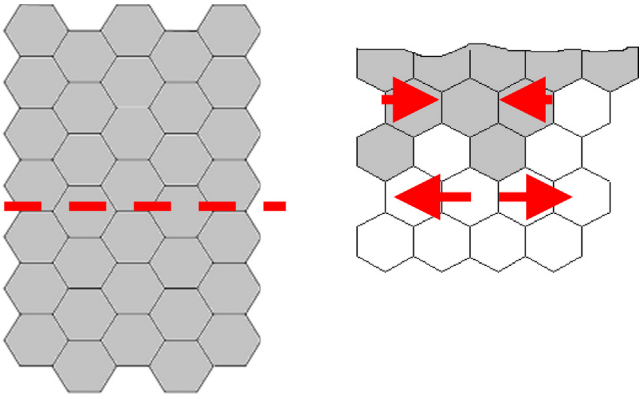

Fig. 1 Complete transformation of tetragonal to monoclinic due to water penetration (Arrow show the nature of stress).

$$\left[Zr_4(OH)_8(H_2O)_{16}\right]^{8+} \rightarrow \left[Zr_4(OH)_{8+X}(H_2O)_{16-X}\right]^{(8-X)} + XH^+ \quad (3)$$

The aforementioned equation clearly shows that zirconia sol has an H^+ or larger concentration of OH^- ion shortage at basic pH levels. According to Liu et al. (Liu et al., 1998), incorporation of Na^+ (which comes from NaOH) into surface-vacant sites also aids in the creation of t-ZrO_2.

All mixtures were then properly washed with DI water and dried at 60 °C. Fig. 2 depicts a schematic illustration of eggshell-mediated zirconia. This is the first study on the direct synthesis of zirconia utilizing eggshells addition. Eqs. (4)–(6) can be used to explain a potential growth mechanism and the impact of eggshell content on the crystal structure.

$$Zr(OH)_4 + 7H_2O + 2HCl \rightarrow \left[Zr(OH)_4\right]_{sol} + 7H_2O \quad (4)$$

$$\left[Zr(OH)_4\right]_{sol} + 7H_2O \overset{Stirring+Eggshells+membrane}{\rightarrow} Zr^{4+} + (4OH^-) + 7H_2O \quad (5)$$

With removal of OH ions

$$Zr^{4+} + O^{2-} \rightarrow ZrO_2 \quad (6)$$

2.2. Characterizations

X-ray diffractometer (XRD) was utilized to examine zirconia nanoparticles at varying eggshell content. The scanning range was 20 to 70°, with 0.05° intervals. Using a confocal Raman spectrometer, the further phase change and confirmation were carried out. Scanning electron microscopy (SEM) and field emission scanning electron microscopy (FE-SEM) were used to investigate the morphology of zirconia at various eggshell contents and magnifications. Vickers nano-indenter was first used to examine the models' toughness in order to make an analysis. Thermo-Fisher ESCLAB performed the XPS.

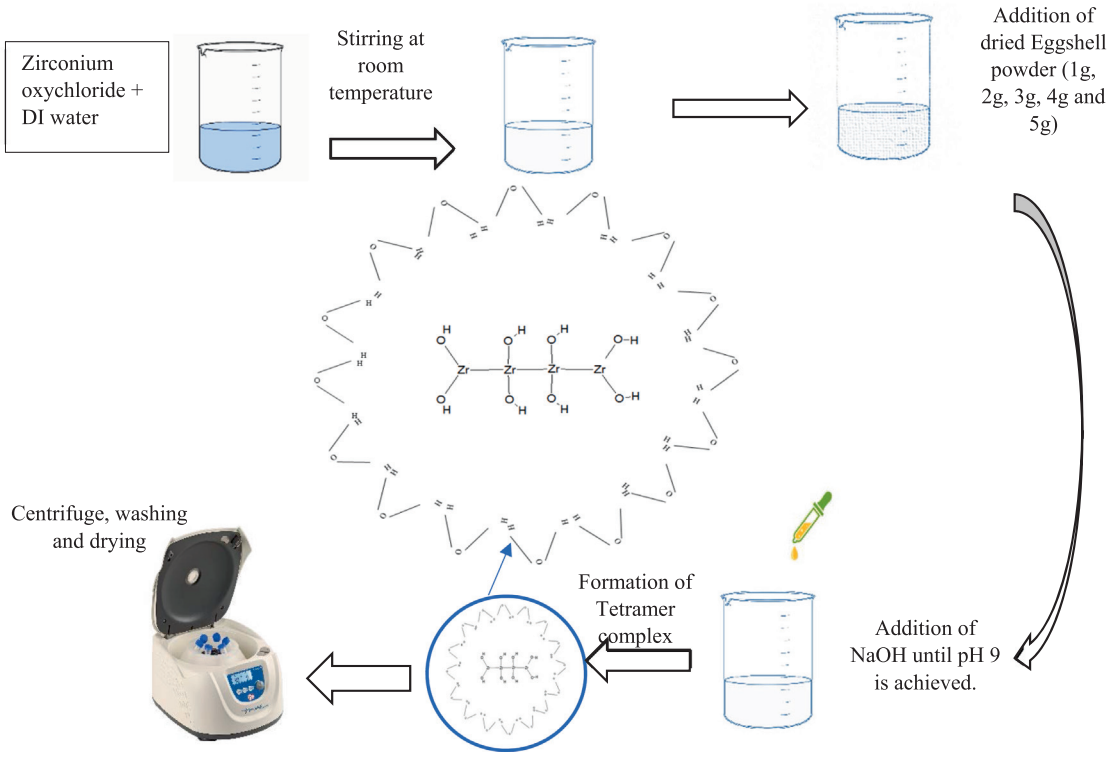

Fig. 2 Schematic representation of eggshell added zirconia nanostructures.

2.2.1. Biodegradation study

The degradation study of eggshell added zirconia was carried out in phosphate buffered saline (PBS) with major constituent lysozyme. Lysozyme mainly responsible for in-vivo degradation of scaffolds. Eggshell added zirconia nanoparticles were soaked in 10 mg/L of PBS for five different intervals 12, 24, 36, 48 and 72 h. Zirconia nanostructures with eggshell added were inspected for degradation both before and after soaking in PBS. DI water was used to clean zirconia nanostructures, and after soaking, they were separated. Samples were dried for 48 h after separation to get rid of any remaining water. The formula found in Eq. (7) (Yoshioka et al., 2008) was used to calculate the weight loss of thoroughly cleaned nanostructures:

$$Weightloss(\%) = \frac{W1 - W2}{W1} \times 100 \quad (7)$$

where,

$W1$ = Weight before soaking.
$W2$ = Weight after soaking.

2.2.2. Antioxidant study

The antioxidant study is very important for bio-materials and implants. Phase pure t-ZrO_2 prepared at 5 g of eggshell content was analyzed for radical scavenging ability. DPPH (1, 1, diphenyl-2-picryl hydrazyl) assay to study the antioxidant properties of prepared samples. The main mechanism involve in antioxidant phenomenon is de-colorization (purple to pale yellow) due to neutralization process. The optimized nanoparticles were added in DPPH and methanol solution. The whole mixture was placed in dark room at 37 °C for 30 min. The measurements were confirmed by de-colorization and by measuring absorbance peak at ~ 517 nm. The percentage scavenging activity was measured by using Eq. (8) (Goujon et al., 2021);

$$Freeraddicalscavengingactivity(\%) = \frac{A_{Blank} - A_{Sample}}{A_{Blank}} \times 100 \quad (8)$$

2.2.3. In-Vitro bio-mineralization study

In vitro study of bio-mineralization of the eggshell added zirconia was carried out through SBF (simulated body fluids) studies. For this purpose, the sample was designed in the shape of disc (13 mm diameter) by using hydraulic press and SBF was prepared according to the proposed strategy by Kokubo et al. (Kokubo et al., 1990). Sterilized plastic containers were used to keep SBF solutions and standard incubator was utilized for incubation at temperature 37 °C with proper shaking at 40 rpm. The specimens were kept completely immersed in SBF throughout the study and SEM analysis was performed after 1, 2, 3, 4, and 5 days.

3. Results and discussion

3.1. Structural study

The current study is carried out to compare different eggshell content on zirconia stabilization. Dried eggshell powder is added into zirconia sols and dried at relatively low temperature. Fig. 3 depicts the XRD patterns of eggshell added zirconia aided by sol–gel method.

The peaks are corresponding to (1 1 1), (0 0 2), (1 1 2), (3 1 1) and (2 2 2) planes of t-ZrO_2 [JCPDS card no. 17–923. Samples synthesized at relatively low eggshell content (1 g and 2 g) exhibit amorphous nature as shown in Fig. 3a and b. Samples show hump around 30° gives an indication of t-ZrO_2. Tyagi et al. (Tyagi et al., 2006) observed same result at 300 °C but here we obtained under as-synthesized conditions. This is known as metastable state of zirconia. As eggshell content increases up to 3 g sharp peaks are observed corresponding to t-ZrO_2. Further increase in eggshell content up to 5 g characteristic peak becomes sharp which means eggshell content enhances the t-ZrO_2 growth. The main reason behind this crystallinity and phase purity is eggshell content cause rapid heating during synthesis and strengthening the tetragonal phase.

The XRD data of eggshell added zirconia further elaborated by Gaussian fitting. Different parameters such as Full width and half maximum (FWHM), center gravity and Area IntgP are calculated. For 1 g and 2 g of eggshell content (Fig. 4a and b) amorphous or humps are observed with FWHM for at 2θ = 30.26486° is 1.14813 and 2θ = 30.859° is 2.8533 respectively. Further increase in eggshell content to 3 g, a slight shifting in angles has been observed and intense tetragonal characteristic peak is observed at 2θ = 30.10972°. FWHM observed for 3 g is 1.06187 (Fig. 4c). The intensity of tetragonal characteristic peak increases up to 5 g at 2θ = 30.1096°. When comparing eggshell contents of 1 g and 2 g, FWHM decreases while a phase change is seen. The FWHM diminishes once the tetragonal concentration reaches 100%, confirming the crystallinity of the t t-ZrO_2. In addition to displaying typical peaks, Gaussian fitting also displays the Area IntgP of each peak. The areas of the tetragonal characteristic peaks at 3 g, 4 g, and 5 g of eggshell content are 42.95479, 49.86866, and 53.13974, respectively. This indicates that the tetragonal content becomes stronger as eggshell content increases. The crystallite size was determined using Scherrer's formula given in Eq. (9) (Cullity, 1956);

$$D_{hkl} = \frac{0.9\lambda}{(FWHM)Cos\theta} \tag{9}$$

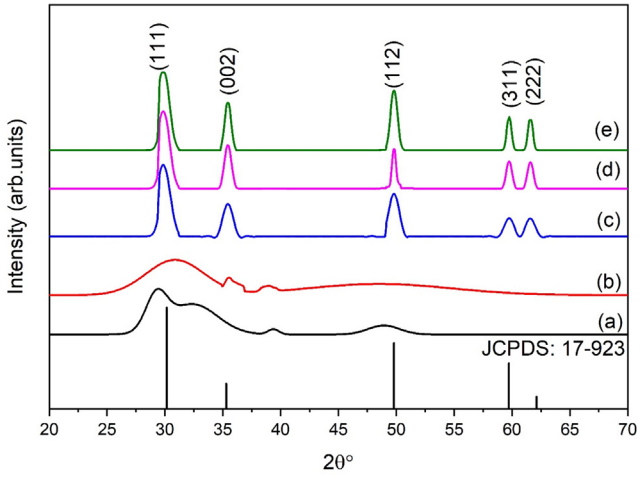

Fig. 3 XRD patterns of zirconia at different eggshell content (a) 1 g, (b) 2 g, (c) 3 g, (d) 4 g and (e) 5 g.

$$\delta = \frac{1}{D^2} \tag{10}$$

where,

D_{hkl} = Crystallite size.

λ = 1.5406 Å.

Crystallite size contain two different regions as shown in Fig. 5a. As metastable phase transforms to t-ZrO_2 crystallite size decreases. When the eggshell content reaches 3 g, the crystallite size increases. Suitable eggshell content works as surfactant and stops further phase transformation. In fact, stabilization of phase occurs with higher content. After stabilization a slight increase in crystallite size has observed which is due to nuclei emergences. Dislocation density was calculated by using Eq. (10). Few dislocation lines have been observed for eggshell added zirconia.

For phases of zirconia unit cell volume have strongly impact. Slight shrinkage in volume causes this transformation. Unit cell volume of ZrO_2 nanostructures is determined using Eq. (11), (Cullity, 1956) and are plotted in Fig. 5b.

$$V_{Tetragonal} = a^2c \tag{11}$$

Unit cell of zirconia nanostructures prepared by eggshells additives shows a drastic decrease with eggshell addition. Literature suggests that 3 to 5% decrement in volume causes phase transformation. Inset of Fig. 5b inset shows the variation in X-ray density. Higher X-ray density (~5.98 g/cm^3) has been perceived eggshell added zirconia samples. X-ray density is employed to calculate the porosity of the samples. Calculations revealed that relatively lower porosity has been observed in phase pure t-ZrO_2 [Fig. 5c]. X-ray density and porosity of ZrO_2 nanostructures was determined by Eqs. (12) and (13) (Cullity, 1956).

$$\rho = \frac{1.66042\Sigma A}{V} \tag{12}$$

Where a, b, and c are lattice quantities, and A is the sum of all atoms' atomic weights in a unit cell.

$$Porosity(\%) = 1 - \frac{\rho_{observed}}{\rho_{Theoretical}} \times 100 \tag{13}$$

2D structures for sample synthesized at 3 g of eggshell content is shown in Fig. 6. Fig. 6 shows the coordination of 2 cations. Each cation is now coordinated by two interpenetrating tetrahedra, an inner slightly compressed tetrahedron, and an outer elongated tetrahedron (Limbu, 2022). The bond length of Zr-O is 2.0932 Å and they are bonded covalently.

3.2. FTIR analysis

Functional group analysis of pure eggshell is illustrated in Fig. 7. FTIR spectrum of eggshell consists of four main groups: O—H, N—H, C—O and C—O—C. O—H bonds normally forms from alcohol and hydrogen group observed at 1630 cm^{-1}. N—H bond comes from amides present in fibers of eggshell. Two strong bonds observed at 887 cm^{-1} and 1400 cm^{-1} are C—O stretching from calcium carbonate which is major content in eggshell (Tizo et al., 2018). Another weak band observed around 1087 cm^{-1} representing the starching from sodium alginate (Lakouraj et al., 2014).

Fig. 7 represents the FTIR analysis of eggshell added zirconia. At lower eggshell content (1 g) one distinct band at

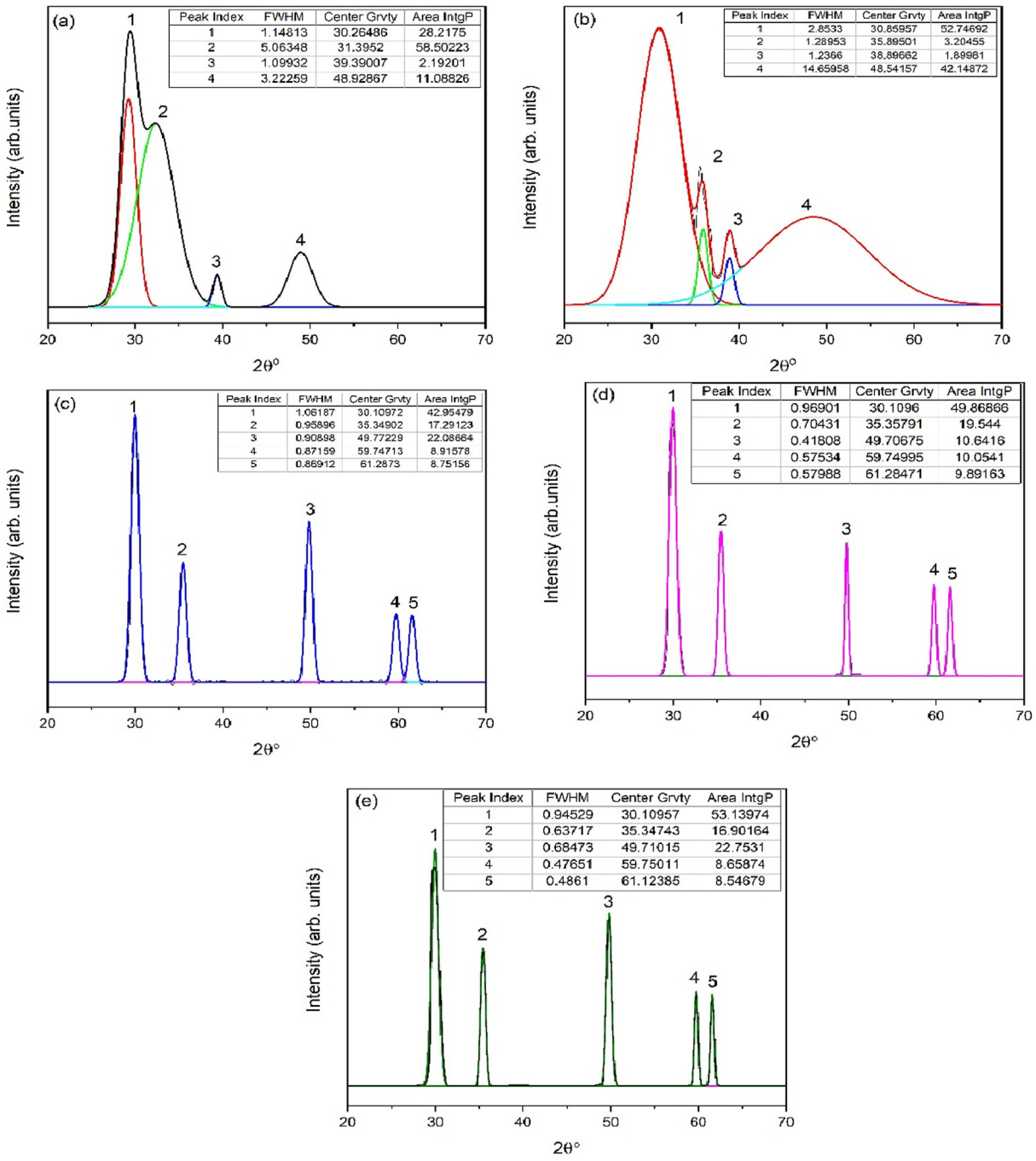

Fig. 4 Corresponding XRD fitted diagram of eggshell added zirconia (a) 1 g, (b) 2 g, (c) 3 g, (d) 4 g and (e) 5 g.

610 cm^{-1} is observed pertained to m-ZrO_2 [Fig. 7a]. Another weak band with a peak at 750 cm^{-1} is also assigned to Zr-O vibrations of t-ZrO_2 (Lee et al., 2023). The band at $\sim$ 887 cm^{-1}correlate to the C—O vibration (Ren et al., 2023). 2 g of eggshell content causes vibration of m-ZrO_2 weakened. A similar observation was reported by Chen et al. (Chen et al., 2005) for mixed phases of zirconia nanostructures. As eggshell content increases up to 3 g a clear band was observed at 460 cm^{-1} which is assigned to t-ZrO_2 [Fig. 7c). For this sample, no peak related to m-ZrO_2 is observed which further confirms the phase purity of t-ZrO_2. Wh further increase in additive content t-ZrO_2 bands strengthen which is in good agreement to XRD data. When an organic additive is used during synthesis, carbon related bands are found in the region of 1000–1200 cm-^{1}. The band at 1130 cm^{-1} is therefore attributed to C—C stretching vibrations. The presence of "carboxylates," which include contributions from the vibrations of aromatic and aliphatic carboxylates, is being revealed by this spectral band. The precise absorption for each carbohydrate is determined in the range from 1000 to 1200 cm^{-1} (Adina et al., 2010; Jayakumar et al., 2011; Almulaiky et al., 2021). Stretching vibrations occur between 1400 and 1600 cm^{-1} C═C (aromatic ring). Although there are two or three aromatic ring bands in

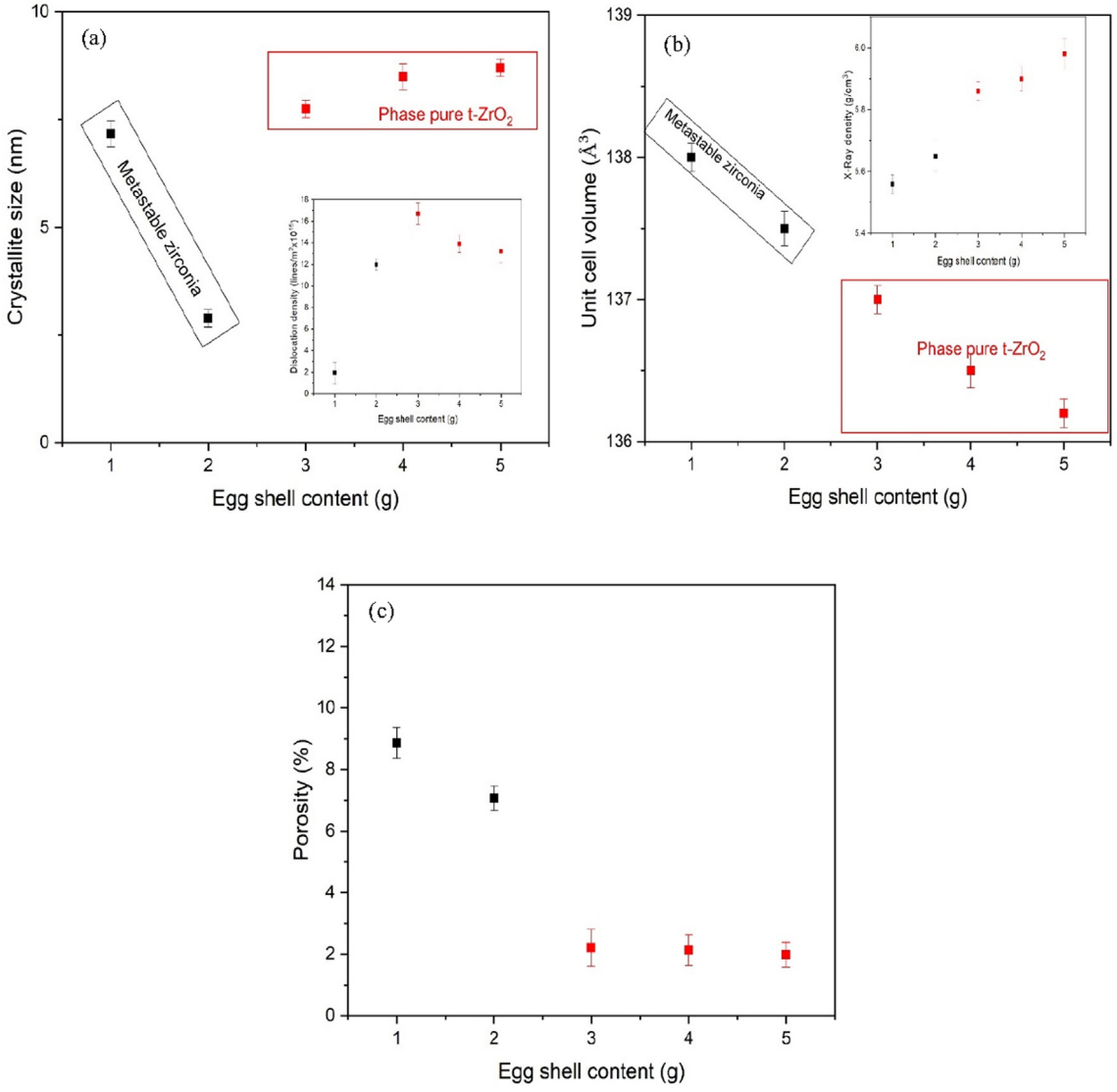

Fig. 5 (a) Crystallite size, (b) Unit cell volume (c) Porosity of eggshell added zirconia. Inset (a) shows the dislocation lines/m^2 and inset (b) X-rays density with eggshell content.

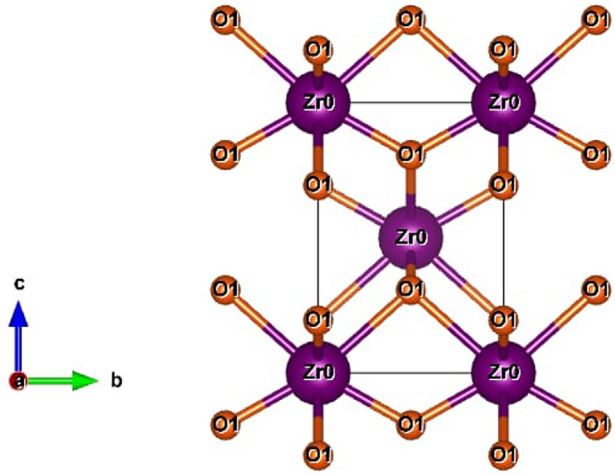

Fig. 6 2D structures of zirconium oxide nanopowder at eggshell content 5 g.

this region, the strongest one was found at about 1400 cm^{-1}. According to the literature (Majid et al., 2022; Tantala et al., 2019), the band at around 1400 cm^{-1} is attributed to an aromatic ring, which comes from an organic ingredient called eggshell. The OH bonds bending and stretching vibrations brought on by absorbed water molecules are responsible for the bands seen at 1630 and 3400 cm^{-1} (Barkat et al., 2022; Xiao et al., 2019).

3.3. RAMAN analysis

Figure 8 (a-b) represents the RAMAN spectra of eggshell added zirconia. There is no sharp peak of monoclinic phase in all samples. However, at relatively low content of eggshell added zirconia (1 g and 2 g) a hump or trace at 332 cm^{-1} are corresponding to B_g mode of monoclinic zirconia (Bhujel et al., 2021). The intensity of this trace decreases with eggshell content. A broad peak at 642 cm^{-1} along with two characteristic tetragonal peaks are observed, even at low eggshell con-

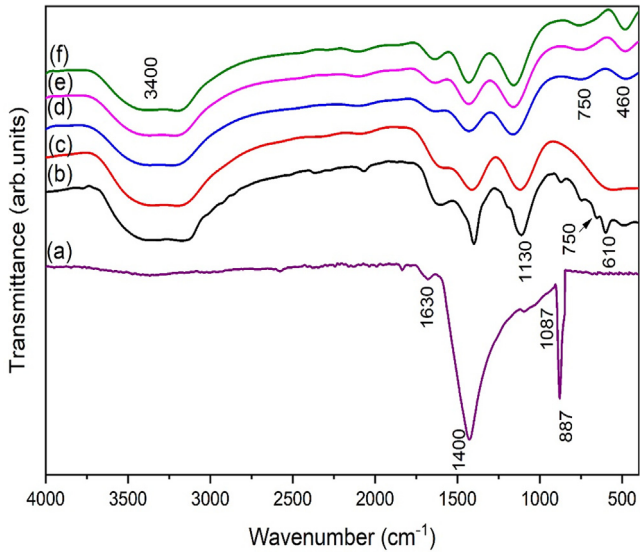

Fig. 7 FTIR of (a) Egg shell and eggshell added zirconia for (b) 1 g, (c) 2 g, (d) 3 g, (e) 4 g and (f) 5 g.

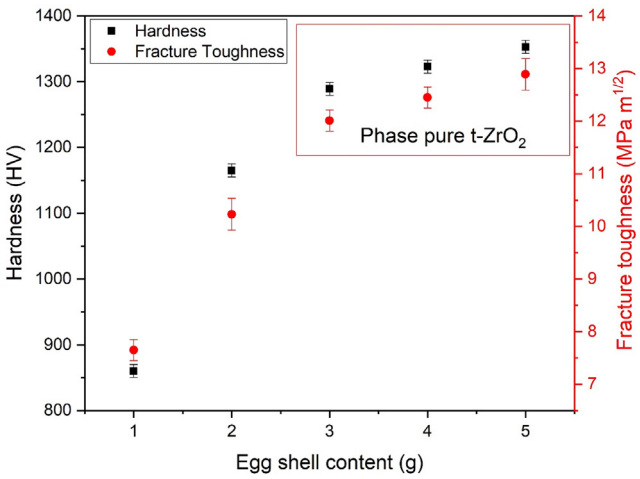

Fig. 9 Hardness and fracture toughness of eggshell added zirconia.

tent. RAMAN analysis further confirms the metatability of t-ZrO_2 (transformation stage to phase pure t-ZrO_2). As eggshell content reaches to 3 g, monoclinic phase diminished and phase pure t-ZrO_2 is confirmed by presence of 3 distinguished peaks at 146 cm^{-1} and 264 cm^{-1} and 642 cm^{-1}. It can be depicted from Fig. 8b the intensity of tetragonal RAMAN bands increases with eggshell content which further confirms that strengthening of t-ZrO_2.

RAMAN spectra can used to calculate phase fraction by following Eq. (14) (Guo et al., 2018; Clarke and Adar, 1982; Bashir et al., 2022).

$$V_t = \frac{0.97[I_t(146) + I_t(264) + I_t(642)]}{0.97[I_t(146) + I_t(264) + I_t(642)] + 0.97[I_m(332) + I_t(264) + I_t(642)]} \quad (14)$$

where,

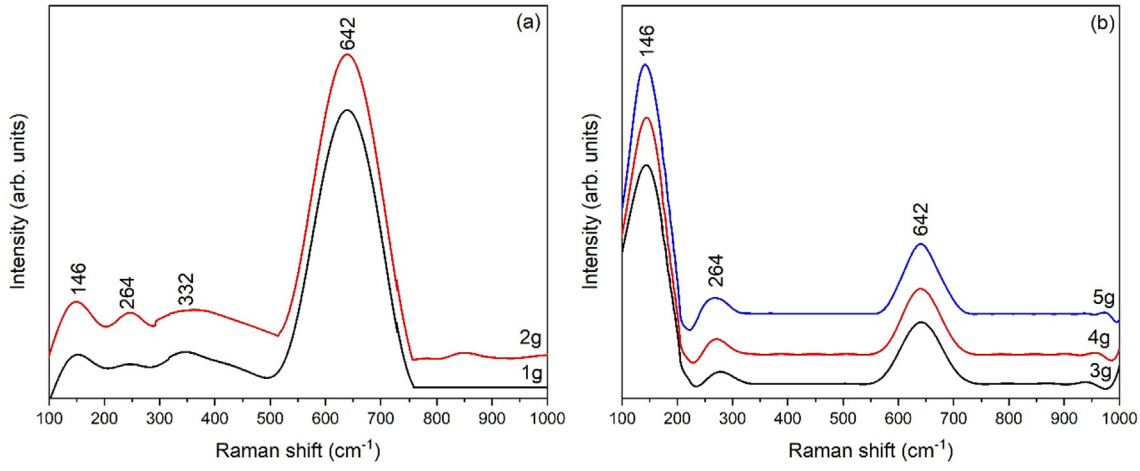

Fig. 8 RAMAN spectra of gelatin added zirconia (a) 1 g and 2 g, (b) 3 g, 4 g and 5 g.

Table 2 Phase fractional ratio and Hardness (HV) of eggshell added ZrO_2.

Eggshell content (g)	t:m	Hardness Vickers(HV) at constant load (5 N) and time (10S)	Fracture Toughness (MPa.$m^{1/2}$)	Zirconia Phase
1	11:89	860 ± 5	7.650 ± 2	Metastable zirconia
2	95:05	1165 ± 5	10.23 ± 2	Metastable zirconia

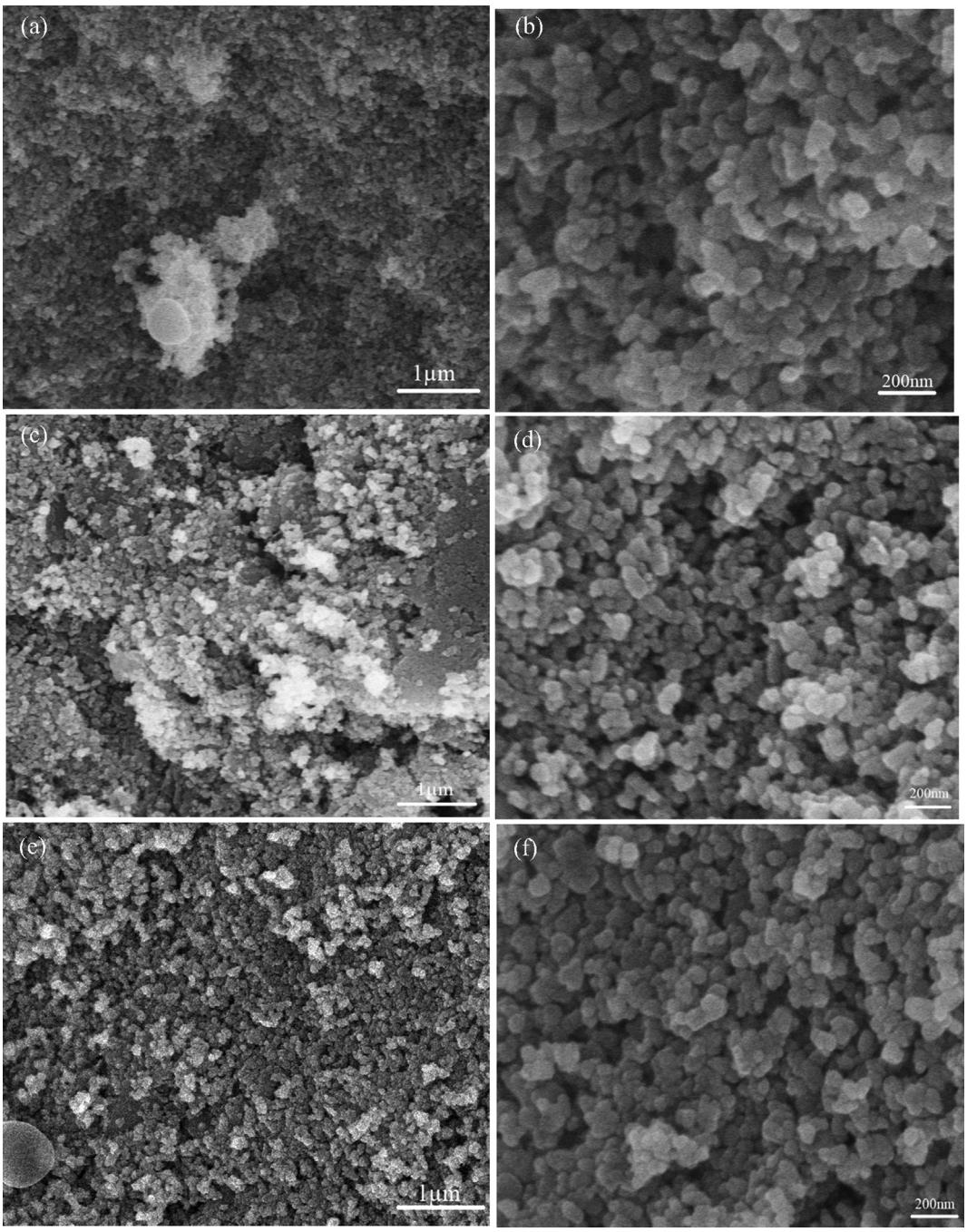

Fig. 10 SEM images of eggshell added zirconia at different eggshell content (a) 3 g, (b) Magnified view at 3 g, (c) 4 g, (d) Magnified view at 4 g, (e) 5 g, and (f) Magnified view at 5 g.

I_t = Intensity of t-ZrO_2.
I_m = Intensity of m-ZrO_2.

The proportion of tetragonal phase in eggshell added zirconia is 11%, 95%, 100%, 100% and 100% for 1 g, 2 g, 3 g, 4 g and 5 g eggshell added zirconia [Table 2].

3.4. Hardness and fracture toughness

As mentioned earlier, eggshell are added in zirconia with aiming strengthen and stabilizing it. Hardness of the samples were perceived by Vickers-Nano-Indenter. Hardness of the samples is correlated with density. As density of the samples increases [Inset Fig. 5b] hardness shows a steep increase. Maximum hardness $\sim$ 1389 has been achieved after obatining phase pure t-ZrO_2. Zirconia with different phases poses different value of hardness and fracture toughness. As eggshell contents changed, so densities of the prepared samples. This had to do with the intricate microstructure. The microstructure of the samples prepared at 5 g and 3 g had fewer pores than that of prepared at 1 g. Samples prepared with 1 g which had a more pronounced presence of the monoclinic phase and high porosity. This came about as a result of the altered density and

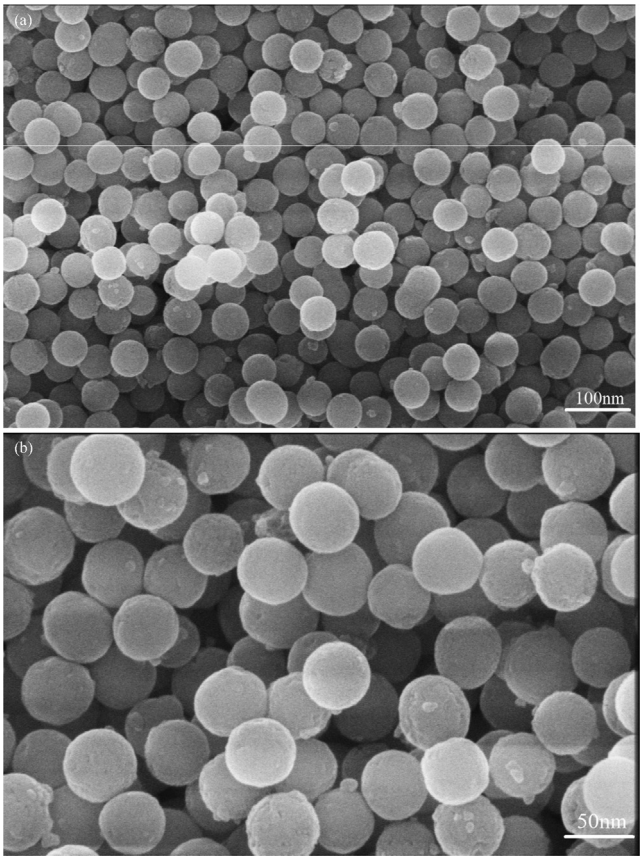

Fig. 11 FE-SEM images of eggshell added zirconia (a) 5 g, (b) Magnified view at 5 g.

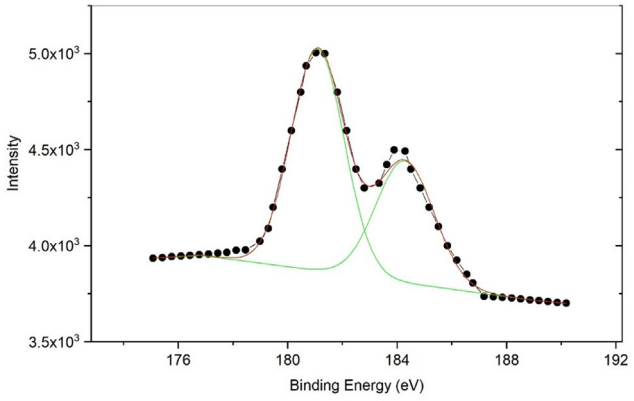

Fig. 12 XPS spectrum of 5 g egg shell added zirconia.

microstructure. Higher density and finer grains were made possible by the presence of eggshell content.

Table 2 summarizes the results of hardness in HV. Facture toughness of the samples is calculated using crack length formed during indentation. Ten measurements were done to satisfy the standard JIS R 1607 (JIS R, 1607). For fracture toughness calculations usually three techniques are used (1) Palmqvist cracks, (2) half-penny crack and (3) curve-fitting. The selection of technique is based on c/a ratio suggested by most cited article (Jenkins and Snyder, 1996). Generally, it is assumed that if c/a less than 2 Palmqvist model is employed (Moradkhani et al., 2013; Ponton and Rawlings, 1989).

The fracture toughness, K_{Ic} (MPa $m^{1/2}$), was calculated using the equation given by Niihara et al. (Niihara et al., 1982) for the Palmqvist cracks.

$$K_{Ic} = 9.052 \times 10^{-3} H^{3/5} E^{3/5} d.c^{-1/2} \quad (15)$$

where

H = Hardness (MPa).
E = Young's modulus (210,000 MPa).
d = Average diagonal line length of the indentation.
c = Average length of the Palmqvist cracks.

Different crack length leads to different fracture toughness. The values are summarized in Table 2 and plotted in Fig. 9. Hardness of the samples and fracture toughness show the three distinct regions is according to XRD analysis. Maximum fracture toughness is observed at 5 g of eggshell content. Generally, grain size and density are influencing parameters for hardness and hence for fracture toughness. Phase purity, non-agglomerated structure, low porosity and high density results in high value of hardness. Comparatively low value of fracture toughness is due to phase transformation, as can be seen in Fig. 3. Regarding fracture toughness, it was demonstrated that the eggshell addition improves fracture toughness. Moreover, it is interesting to note that there is small porosity observed in microstructures which helps to reduce crack formation. Absence of crack is one of the cause of strengthening the material.

The connection between porosity and hardness can be understand by following Eq. (16) (Poole, 2004):

$$\mathrm{HV} = Hv = H_o e^{-bP} \quad (16)$$

where,

H_o = Hardness of material.
b = Constant.
P = Porosity.

Above Eq. (16) confirms that porosity and density are basic parameters to decide the strength of a material. Low porosity and smaller crystallite size causes high HV values as shown in Table 2. Hardness of the samples improves with decrease in phase purity and crystallite size as observed in XRD data (Figs. 3 and 5a).

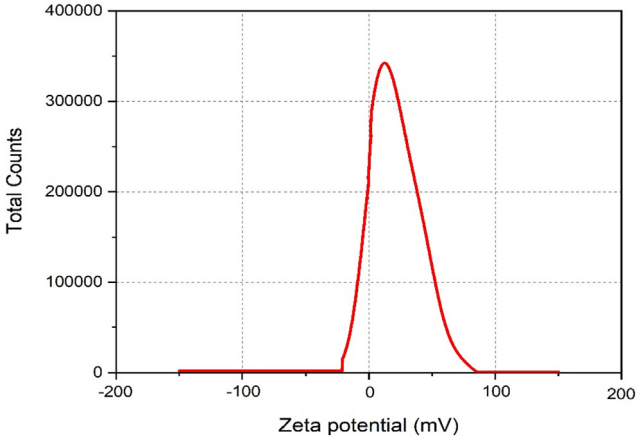

Fig. 13 Zeta Potential of 5 g egg shell added zirconia.

Table 3 Variation in Hardness and weight loss of eggshell added zirconia after Biodegradation test.

Time intervals (h)	Weight loss (%)	Hardness (HV)
12	0.95 ± 0.1	1375 ± 5
24	1.25 ± 0.1	1335 ± 5
36	1.56 ± 0.1	1305 ± 5
48	2.7 ± 0.2	1283 ± 5
72	6.29 ± 0.1	1250 ± 5

3.5. Morphological study

Fig. 10(a and b) shows that SEM images for 3 g of eggshell content. Images reveal some content of porosity and particle agglomeration. Comparing Fig. 10a and 10c, it is observable that by increasing eggshell content, the contribution of particles was effectively constant, and the dispersion is good. Sample prepared at 4 g of eggshell content reveals the high density is consistent with earlier calculation [Fig. 5-inset]. The size of the nanostructures and phase fraction depends upon the synthesis route. Almost spherical nanoparticles are achieved with size ranges 40– 50 nm. The porosity of the samples decreases and reaching a minimum value at 5 g of eggshell content [Fig. 10 e and f] is consistent with XRD data calculations [Fig. 5]. Some content of porosity is yet available which is required for scaffold to form bonding with body tissues.

In Fig. 10f, some content of agglomeration and interconnected nanostructures have been observed. The formation of nanoparticles in the crystalline structure is due to the presence of hydroxyl ions formed during sol–gel synthesis (Yeşil Acar et al., 2022). Nanoparticle morphology further analyzed by FE-SEM as shown in Fig. 11 a and b. FE-SEM images further confirms the size and well dispersed spherical formation of zirconia nanoparticles. Eggshell works as a surfactant along with body compatible properties and prevents the agglomeration phenomenon which is one of the cause of monoclinic (less strength) phase. As discussed earlier [Fig. 1], cracks formation

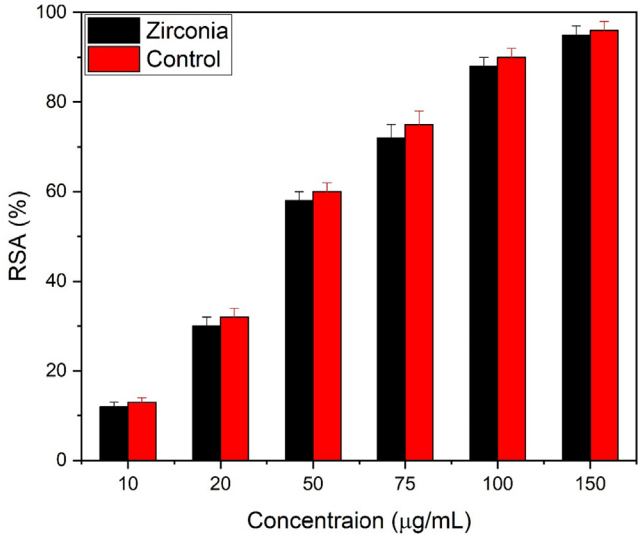

Fig. 14 Antioxidant study of zirconia nanoparticles at different concentrations.

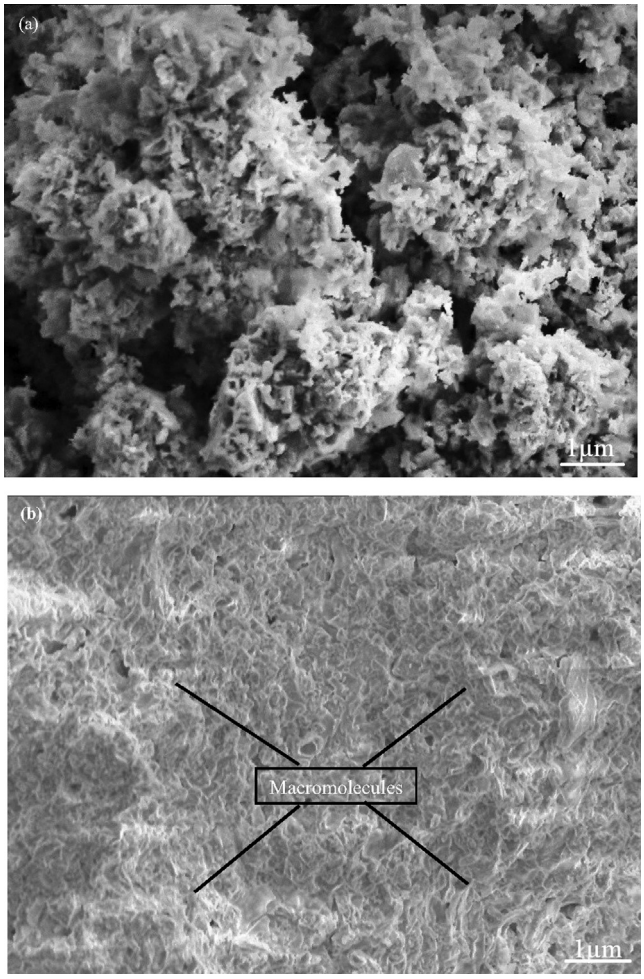

Fig. 15 SEM images of the mineralization of the eggshell added zirconia scaffolds after (a) 1 week (b) 5 weeks.

caused by water molecules adsorption. Water adsorption is the cause of volume expansion and stresses. These stresses ultimately result in monoclinic phase. Presence of surfactant (eggshell) coats the surface and reduces the water adsorption.

3.6. XPS study

Further evidence of t-ZrO_2 was obtained by XPS spectrum of eggshell added zirconia Fig. 12 shows the XPS spectrum for 5 g of eggshell content. The sample exhibited two main t-ZrO_2 peaks at 182 eV and 184 eV in the Zr3d XP spectrum pertaining to $Zr3d_{5/2}$ and $Zr3d_{3/2}$ in Zr–O, respectively (Zhu et al., 2018).

3.7. Zeta potential

The major challenge for the bio-applications of metal oxide nanoparticles is their stability issue in aqueous medium. Usually nanomaterials in powder form are used in biological applications, especially in toxicological studies which require highly dispersible materials for in vitro as well as in vivo experiments. Moreover, stable and highly dispersible nanoparticles gives better and versatile interface, which further helps in better interaction with biomaterials.

The stability criteria of ZrO_2 nanoparticles prepared at 5 g of eggshell content is calculated for zeta potential range +30 mV to −30 mV. Fig. 13 depicts zeta potential distributions of ZrO_2nanoparticles illuminated by 1,064 nm in distilled water solution. The zeta potential value of distilled water solution is 54.12 mV, which indicates the stable nanoparticles with very less agglomeration in the solution.

3.8. In-vitro biodegradation study

After achieving phase pure t-ZrO_2 biodegradation study was carried out for and variation in weight and hardness were examined. Sample synthesized at 5 g of eggshell content was immersed in phosphate buffered saline (PBS) which is containing lysozyme for different time intervals (12, 24, 36, 48 and 72 h). Slight decrease in weight and loss has been observed even after 72 h of immersion. It can be seen that although hardness of the samples decreases to 1250 HV but it is still suitable for bone implantations. The observed values determined by Eq. (7) are accessible in Table 3.

The outcome demonstrates that scaffold weight steadily decreased during degradation with an increase in the PBS incubation time. However, biocompatibility of the synthesized eggshell added zirconia impede the regular cell functions. Biocompatibility and degradation rate play an important role for maintaining the function of bone implantation. A moderate degradation rate is required for new bone formation. Very slow degradation rate can impede the formation of new bon whereas, very high degradation rate cannot support the defect site. The faster hydrolysis degradation, or weight loss in composite scaffolds is due to higher water molecules absorbed by scaffolds (Sousa et al., 2008). It is earlier reported for perfect bone formation degradation rate must be less than 2% per day (Zeng et al., 2020). Evidently synthesized scaffolds representing the desired degradation rate for new bone formation. Usually required size and shape of the scaffolds depends upon the site where to be implanted. Here well-dispersed and spherical nanoparticles are required to meet the clinical criteria of bone implants.

3.9. Antioxidant study

Eggshell added zirconia nanoparticles were studied for antioxidant activity as shown in Fig. 14. The activity were studied at 10, 20, 50, 75, 100 and 150 μg/mL concentration of zirconia nanoparticles. The percentage increases with concentration of zirconia nanoparticles. The addition of nanoparticles coating the surface and enhances the free scavenging radical activity (RSA) of zirconia. The reason why the antioxidant properties of eggshell are enhanced, is due to the encapsulation phenomenon. Eggshells normally contain polyphenol compounds which naturally enhance the antioxidant properties.

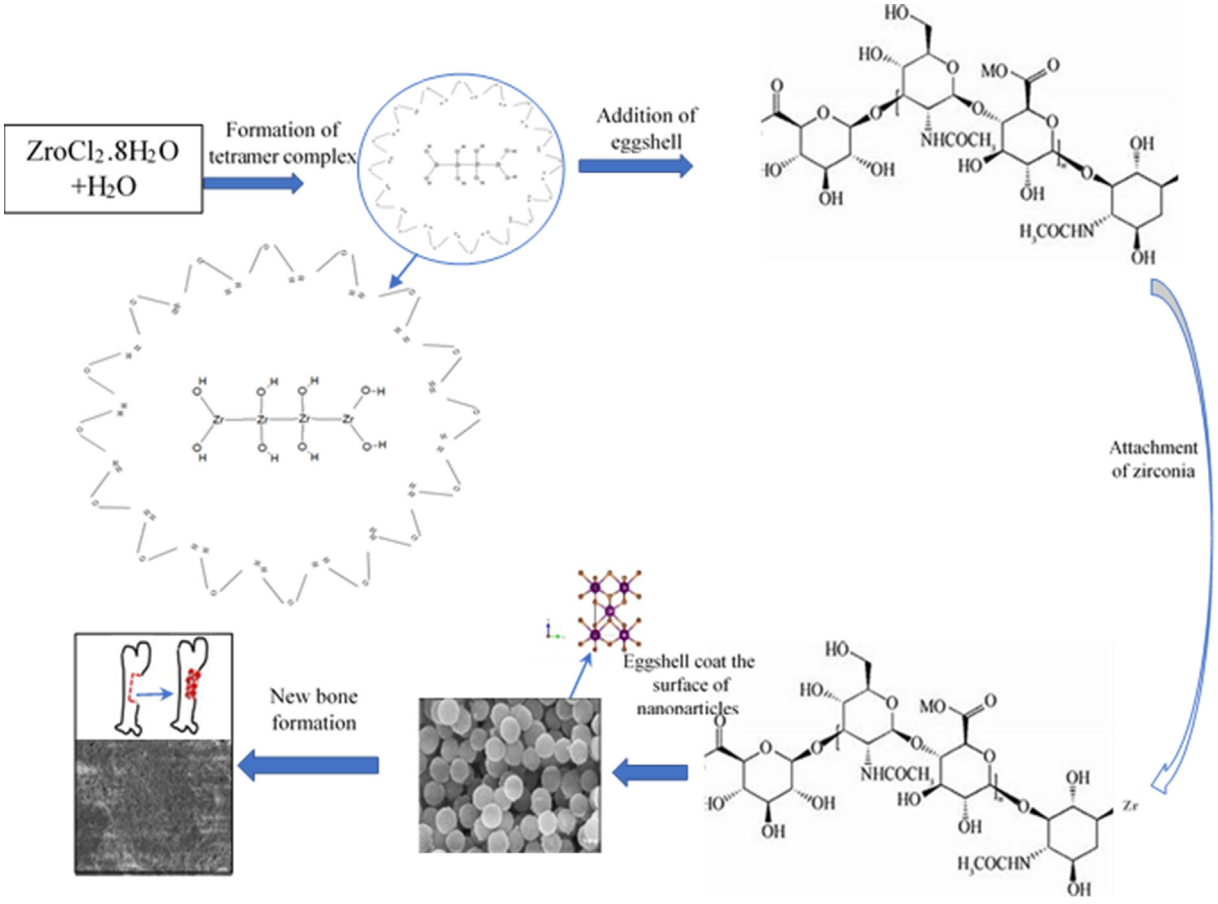

Fig. 16 Chemical structure formulation and application schematic of eggshell added zirconia.

Moreover, eggshells membrane contains collagen proteins an ideal natural ingredient, well-known to have an antioxidant activity and proliferation of fibroblast cell (Chotphruethipong et al., 2021). Eggshell added zirconia nanoparticles shows 96% of RSA activity which is greater as compared to literature (Tabassum et al., 2021), which means eggshell enhances the antioxidant activity. An antioxidant study carried out by Al-Fahdawi et al. (Al-Fahdawi et al., 2015) presented that sulfated zirconia shows 55% activity. Another antioxidant study of green synthesized zirconia showed the RSA ~ 85 % at 158.15 µg/mL (Balaji et al., 2017).

3.10. In-vitro bio-mineralization study

In vitro bio-mineralization study was carried out for 5 g of eggshell added zirconia for 1, 2 3, 4, and 5 weeks in SBF and were analyzed under SEM. Deposition of hydroxyapatite on the zirconia nanoparticles surfaces confirms the production of new bone. After 1 week less mineralization was observed [Fig. 15a] while after 5 weeks all pores were filled and minerals were deposited on the surface of the scaffolds [Fig. 15b]. Different studies presented that in-vitro mineralization presence of apatite layer on the surface of nanoparticles followed by amount of calcium and phosphorous (Teimouri et al., 2015; Rasheed et al., 2019). Calcium and phosphorous are extracted from eggshell which facilitates the formation of apatite layer. As exposure time increases the thickness of apatite layer increases and flake like interconnected macromolecules with size ranges 0.1 cm to 1 cm are observed. The SEM images revealed that minerals deposition increases with deposition time. The formation of apatite layer on the surface of zirconia nanoparticles suggested the good sign of activity. Bargavi et al. (Bargavi et al., 2020) showed that zirconia reaction with wollastonite form Zr-OH functional groups. These functional groups act as nucleation sites. They correlate their results with XRD obtained after mineralization peak intensity increases with soaking time as observed in present study. Fig. 16 represents the schematic view of formation mechanism and application of egg shell added zirconia.

4. Conclusions

Zirconia nanoparticles were synthesized by sol–gel method at different eggshell contents (1 g, 2 g, 3 g, 4 g and 5 g). XRD results confirmed the establishment of a pure ZrO2 tetragonal phase, at 3 g eggshell content. Further increase in eggshell content resulted in a strengthening phase. Nanoparticles prepared at 3 g contents revealed the high density and high value of hardness due to phase purity. FTIR spectra further confirmed the phase purity with peaks at 460 and 750 cm^{-1}. SEM and FE-SEM images confirmed the well-defined, dense and non-agglomerated spherical nanoparticles. Biodegradation study presented the slight variation in hardness and weight loss after soaking in PBS. Antioxidant study revealed the 96% of RSA activity. In-vitro-mineralization study confirmed the formation of bone.

Funding

Researchers Supporting Project number (RSPD2023R665), King Saud University, Riyadh, Saudi Arabia.

Declaration of Competing Interest

The authors declare that they have no known competing financial interests or personal relationships that could have appeared to influence the work reported in this paper.

Acknowledgments

The authors acknowledge the funding from Researchers Supporting Project number (RSPD2023R665), King Saud University, Riyadh, Saudi Arabia.

References

Adina, C.H., Florinela, F.E., Abdelmoumen, T.A., Carmen, S., 2010. Application of FTIR spectroscopy for a rapid determination of some hydrolytic enzymes activity on sea buckthorn substrate. Romanian Biotechnol. Lett. 15 (6), 5738–5744.

Al-Fahdawi, M.Q., Rasedee, A., Al-Qubaisi, M.S., Alhassan, F.H., Rosli, R., El Zowalaty, M.E., Taufiq-Yap, Y.H., 2015. Cytotoxicity and physicochemical characterization of iron–manganese-doped sulfated zirconia nanoparticles. Int. J. Nanomed. 10, 5739.

Almulaiky, Y.Q., Khalil, N.M., El-Shishtawy, R.M., Altalhi, T., Algamal, Y., Aldhahri, M., Mohammed, M.M., 2021. Hydroxyapatite-decorated ZrO2 for α-amylase immobilization: Toward the enhancement of enzyme stability and reusability. Int. J. Biol. Macromol. 167, 299–308.

Bagbi, Y., Sharma, A., Bohidar, H.B., Solanki, P.R., 2016. Immunosensor based on nanocomposite of nanostructured zirconium oxide and gelatin-A. Int. J. Biol. Macromol. 82, 480–487.

Balaji, S., Mandal, B.K., Ranjan, S., Dasgupta, N., Chidambaram, R., 2017. Nano-zirconia–evaluation of its antioxidant and anticancer activity. *J. Photochem. Photobiol. B*: Biology 170, 125–133.

Bapat, R.A., Yang, H.J., Chaubal, T.V., Dharmadhikari, S., Abdulla, A.M., Arora, S., Kesharwani, P., 2022. Review on synthesis, properties and multifarious therapeutic applications of nanostructured zirconia in dentistry. RSC Adv. 12 (20), 12773–12793.

Bargavi, P., Chitra, S., Durgalakshmi, D., Radha, G., Balakumar, S., 2020. Zirconia reinforced bio-active glass coating by spray pyrolysis: Structure, surface topography, in-vitro biological evaluation and antibacterial activities. Mater. Today Commun. 25, 101253.

Barkat, F., Afzal, M., Khan, B.S., Saeed, A., Bashir, M., Mukhtar, A., Wu, K., 2022. Formation mechanism and lattice parameter investigation for copper-substituted cobalt ferrites from Zingiber officinale and Elettaria cardamom seed extracts using biogenic route. Materials 15 (13), 4374.

Bashir, M., Riaz, S., Kayani, Z.N., Naseem, S., 2018. Synthesis of bone implant substitutes using organic additive based zirconia nanoparticles and their biodegradation study. J. Mech. Behav. Biomed. Mater. 88, 48–57.

Bashir, M., Majid, F., Akram, S., Ali, A., Abdelmohsen, S.A., 2022. Biodegradation of gelatin stabilized tetragonal zirconia synthesized by microwave assisted sol-gel method. J. Mech. Behav. Biomed. Mater. 127, 105070.

Bhowmick, A., Pramanik, N., Jana, P., Mitra, T., Gnanamani, A., Das, M., Kundu, P.P., 2017. Development of bone-like zirconium oxide nanoceramic modified chitosan based porous nanocomposites for biomedical application. Int. J. Biol. Macromol. 95, 348–356.

Bhujel, A., Sapkota, B., Aryal, R.L., Poudel, B.R., Bhattarai, S., Gautam, S.K., 2021. Insight of precursor concentration, particle size and band gap of zirconia nanoparticles synthesized by co-precipitation method. BIBECHANA 18 (1), 1–9.

Chen, Y.-W., Moussi, J., et al, 2016. Zirconia in biomedical applications. Expert Rev. Med. Devices 13 (10), 945–963.

Chen, S., Yin, Y., Wang, D., Liu, Y., Wang, X., 2005. Structures, growth modes and spectroscopic properties of small zirconia clusters. J. Cryst. Growth 282 (3–4), 498–505.
Chevalier, J., Gremillard, L., Virkar, A.V., Clarke, D.R., 2009. The tetragonal-monoclinic transformation in zirconia: lessons learned and future trends. J. Am. Ceramic Soc. 92, 1901–1920.
Cho, J.H., Han, J.S., Yoon, H.I., Yeo, I.S.L., 2023. Effect of phase fraction and grain size on translucency of 3 mol% yttria-stabilized tetragonal zirconia polycrystal. J. Mater. Res. Technol. 25, 1222–1230.
Chotphruethipong, L., Sukketsiri, W., Aluko, R.E., Sae-Leaw, T., Benjakul, S., 2021. Effect of hydrolyzed collagen from defatted Asian sea bass (Lates calcarifer) skin on fibroblast proliferation, migration and antioxidant activities. J. Food Sci. Technol. 58 (2), 541–551.
Clarke, D.R., Adar, F., 1982. Measurement of the crystallographically transformed zone produced by fracture in ceramics containing tetragonal zirconia. J. Am. Ceram. Soc. 65 (6), 284–288.
Cranin, A.N., Schnitman, P.A., et al, 1975. Alumina and zirconia coated vitallium oral endosteal implants in beagles. J. Biomed. Mater. Res. 9 (4), 257–262.
Cullity, B.D., 1956. Elements of X-ray Diffraction. Addison-Wesley Publishing.
Denkewicz, R.P., TenHuisen, K.S., Adair, J.H., 1990. Hydrothermal crystallization kinetics of m-ZrO_2 and t-ZrO_2. J. Mater. Res. 5 (11), 2698–2705.
Fedorenko, N.Y., Abiev, R.S., Kudryashova, Y.S., Ugolkov, V.L., Khamova, T.V., Mjakin, S.V., Shilova, O.A., 2022. Comparative study of zirconia based powders prepared by co-precipitation and in a microreactor with impinging swirled flows. Ceram. Int. 48 (9), 13006–13013.
Firth, F.C., Gaultois, M.W., Wu, Y., Stratford, J.M., Keeble, D.S., Grey, C.P., Cliffe, M.J., 2021. Exploring the role of cluster formation in UiO Family Hf metal-organic frameworks with in situ X-ray pair distribution function analysis. J. Am. Chem. Soc. 143 (47), 19668–19683.
Goujon, G., Baldim, V., Roques, C., Bia, N., Seguin, J., Palmier, B., Beray-Berthat, V., 2021. Antioxidant activity and toxicity study of cerium oxide nanoparticles stabilized with innovative functional copolymers. Adv. Healthc. Mater. 10 (11), 2100059.
Guo, F., Liu, Y., Wang, G., Yi, M., Cai, H., Wang, X., Zhao, X., 2018. Hydrothermal ageing of tetragonal zirconia porous membranes: Effect of thermal residual stresses on the phase stability. Corros. Sci. 142, 66–78.
Hincke, M.T., Nys, Y., Gautron, J., Mann, K., Rodriguez-Navarro, A.B., McKee, M.D., 2012. The eggshell: structure, composition and mineralization. Front. Biosci. 17 (1), 1266–1280.
Hoffmann, O., Angelov, N., Gallez, F., Jung, R.E., Weber, F.E., 2008. The zirconia implant-bone interface: a preliminary histologic evaluation in rabbits. Int. J. Oral Maxillofac. Implants 23 (4), 691–695.
Jayakumar, R., Ramachandran, R., Kumar, P.S., Divyarani, V.V., Srinivasan, S., Chennazhi, K.P., Nair, S.V., 2011. Fabrication of chitin–chitosan/nano ZrO_2 composite scaffolds for tissue engineering applications. Int. J. Biol. Macromol. 49 (3), 274–280.
Jenkins, R., Snyder, R.L., 1996. Introduction to X-ray Powder Diffractometry. John Wiley & Sons, NY.
Jin, G.Z., Kim, H.W., 2018. Efficacy of collagen and alginate hydrogels for the prevention of rat chondrocyte dedifferentiation. J. Tissue Eng. 9. 2041731418802438.
JIS R 1607: Testing Methods for Fracture Toughness of High Performance Ceramics, Japanese Standards Association, Tokyo, 1990.
Kafi, M., Aktar, M., Phanny, Y., Todo, M., 2019. Adhesion, proliferation and differentiation of human mesenchymal stem cell on chitosan/collagen composite scaffold. J. Mater. Sci. - Mater. Med. 30 (12), 1–12.
Kaizawa, Y., Leyden, J., Behn, A.W., Tulu, U.S., Franklin, A., Wang, Z., Fox, P.M., 2019. Human tendon–derived collagen hydrogel significantly improves biomechanical properties of the tendon-bone interface in a chronic rotator cuff injury model. J. Hand Surg. Am. 44 (10), 899–e1.
Katsube, K., Ochi, M., Uchio, Y., Maniwa, S., Matsusaki, M., Tobita, M., Iwasa, J., 2000. Repair of articular cartilage defects with cultured chondrocytes in Atelocollagen gel. Arch. Orthop. Trauma Surg. 120 (3), 121–127.
Kokubo, T., Kushitani, H., Sakka, S., Kitsugi, T., Yamamuro, T., 1990. Solutions able to reproduce in vivo surface-structure changes in bioactive glass-ceramic A-W3. J. Biomed. Mater. Res. 24 (6), 721–734.
Lakouraj, M.M., Mojerlou, F., Zare, E.N., 2014. Nanogel and superparamagnetic nanocomposite based on sodium alginate for sorption of heavy metal ions. Carbohydr. Polym. 106, 34–41.
Lee, J., Jang, K.B., Lee, S., Mo, C.B., Kim, H.K., Park, K.R., Mhin, S., 2023. Mechanical properties of TiC reinforced MgO–ZrO2 composites via spark plasma sintering. Ceram. Int. 49 (11), 17255–17260.
Limbu, S., 2022. Investigation of crystal structure confinement and optical attributes of monoclinic–tetragonal Zirconia nanocrystals via chemical co-precipitation technique. Bull. Mater. Sci. 45 (4), 182.
Liu, Z., Ji, W., Dong, L., Chen, Y., 1998. Effect of supported Na^+ ions on the texture properties of ZrO_2. J. Solid State Chem. 138 (1), 41–46.
Mahmood, Q., Afzal, A., et al, 2013. Sol–gel synthesis of tetragonal ZrO_2 nanoparticles stabilized by crystallite size and oxygen vacancies. J. Sol-Gel Sci. Technol. 67 (3), 670–674.
Majid, F., Bashir, M., Bibi, I., Raza, A., Ezzine, S., Alwadai, N., Iqbal, M., 2022. ZnO nanofibers fabrication by hydrothermal route and effect of reaction time on dielectric, structural and optical properties. J. Mater. Res. Technol. 18, 4019–4029.
Moradkhani, A., Baharvandi, H., Tajdari, M., Latifi, H., Martikainen, J., 2013. Determination of fracture toughness using the area of micro-crack tracks left in brittle materials by Vickers indentation test. J. Adv. Ceram. 2 (1), 87–102.
Niihara, K., Morena, R., Hasselman, D.P.H., 1982. Evaluation of KIc of brittle solids by the indentation method with low crack-to-indent ratios. J. Mater. Sci. Lett. 1 (1), 13–16.
Okada, M., Taketa, H., Torii, Y., Irie, M., Matsumoto, T., 2019. Optimal sandblasting conditions for conventional-type yttria-stabilized tetragonal zirconia polycrystals. Dent. Mater. 35 (1), 169–175.
Parera, J.M., 1992. Promotion of zirconia acidity by addition of sulfate ion. Catal. Today 15 (3–4), 481–490.
Ponton, C.B., Rawlings, R.D., 1989. Vickers indentation fracture toughness test Part 1 Review of literature and formulation of standardised indentation toughness equations. Mater. Sci. Technol. 5 (9), 865–872.
Poole Jr., C.P., 2004. Encyclopedic Dictionary of Condensed Matter Physics. Academic Press.
Rasheed, T., Bilal, M., Zhao, Y., Raza, A., Shah, S.Z.H., Iqbal, H.M., 2019. Physiochemical characteristics and bone/cartilage tissue engineering potentialities of protein-based macromolecules—a review. Int. J. Biol. Macromol. 121, 13–22.
Redfern, S.E., Grimes, R.W., Rawlings, R.D., 2001. The Hydroxylation of t-ZrO_2 Surfaces. J. Mater. Chem. 11, 449–455.
Ren, L., Liu, S., Huang, S., Wang, Q., Lu, Y., Song, J., Guo, J., 2023. Identification of microplastics using a convolutional neural network based on micro-Raman spectroscopy. Talanta 260, 124611.
Riaz, S., Bashir, M., Naseem, S., 2015. Synthesis of stabilized zirconia hollow nanoparticles: sugar as a template. J. Sol-Gel Sci. Technol. 74 (2), 275–280.
Sanaullah, I., Bashir, M., Batool, T., Riaz, S., Ali, D., Sabri, A.N., Naseem, S., 2021. Tangerine mediated synthesis of zirconia as

potential protective dental coatings. Mater. Sci. Eng. C 120, 111653.
Shadianlou, F., Foorginejad, A., Yaghoubinezhad, Y., 2022. Fabrication of zirconia/reduced graphene oxide/hydroxyapatite scaffold by rapid prototyping method and its mechanical and biocompatibility properties. Ceram. Int. 48 (5), 7031–7044.
Siddiqui, M.R.H., Al-Wassil, A.I., Al-Otaibi, A.M., Mahfouz, R.M., 2012. Effects of precursor on the morphology and size of ZrO2 nanoparticles, synthesized by sol-gel method in non-aqueous medium. Mater. Res. 15, 986–989.
Son, J.R., Gwon, T.D., Kim, S.B., 2001. Characterization of zirconium sulfate supported on zirconia and activity for acid catalysis. Bull. Kor. Chem. Soc. 22 (12), 1309–1315.
Sousa, R.C., Lobato, J.V., Maurício, A.C., Hussain, N.S., Botelho, C. M., Lopes, M.A., Santos, J.D., 2008. A clinical report of bone regeneration in maxillofacial surgery using Bonelike® synthetic bone graft. J. Biomater. Appl. 22 (4), 373–385.
Tabassum, N., Kumar, D., Verma, D., Bohara, R.A., Singh, M.P., 2021. Zirconium oxide (ZrO_2) nanoparticles from antibacterial activity to cytotoxicity: a next-generation of multifunctional nanoparticles. Mater. Today Commun. 26, 102156.
Takallu, S., Mirzaei, E., Azadi, A., Karimizade, A., Tavakol, S., 2019. Plate-shape carbonated hydroxyapatite/collagen nanocomposite hydrogel via in situ mineralization of hydroxyapatite concurrent with gelation of collagen at ph = 7.4 and 37 c. J. Biomedical Mater. Res. Part B: Appl. Biomater. 107 (6), 1920–1929.
Tantala, J., Thumanu, K., Rachtanapun, C., 2019. An assessment of antibacterial mode of action of chitosan on Listeria innocua cells using real-time HATR-FTIR spectroscopy. Int. J. Biol. Macromol. 135, 386–393.
Teimouri, A., Ebrahimi, R., Emadi, R., Beni, B.H., Chermahini, A.N., 2015. Nano-composite of silk fibroin–chitosan/Nano ZrO2 for tissue engineering applications: Fabrication and morphology. Int. J. Biol. Macromol. 76, 292–302.
Tizo, M.S., Blanco, L.A.V., Cagas, A.C.Q., Cruz, B.R.B.D., Encoy, J. C., Gunting, J.V., Mabayo, V.I.F., 2018. Efficiency of calcium carbonate from eggshells as an adsorbent for cadmium removal in aqueous solution. Sustainable Environ. Res. 28 (6), 326–332.
Tsai, W.T., Yang, J.M., Lai, C.W., Cheng, Y.H., Lin, C.C., Yeh, C. W., 2006. Characterization and adsorption properties of eggshells and eggshell membrane. Bioresour. Technol. 97 (3), 488–493.
Tyagi, B., Sidhpuria, K., Shaik, B., Jasra, R.V., 2006. Synthesis of nanocrystalline zirconia using sol– gel and precipitation techniques. Ind. Eng. Chem. Res. 45 (25), 8643–8650.
Xiao, T., Yuan, H., Ma, Q., Guo, X., Wu, Y., 2019. An approach for in situ qualitative and quantitative analysis of moisture adsorption in nanogram-scaled lignin by using micro-FTIR spectroscopy and partial least squares regression. Int. J. Biol. Macromol. 132, 1106–1111.
Yeşil Acar, Z., Asiltürk, M., Arpaç, E., 2022. Preparation of ceria by combined sol–gel and hydrothermal method: insights from the effects of different bases on the particle size distribution. Chem. Pap. 76 (8), 4927–4939.
Yoshioka, T., Kawazoe, N., Tateishi, T., Chen, G., 2008. In vitro evaluation of biodegradation of poly (lactic-co-glycolic acid) sponges. Biomaterials 29 (24–25), 3438–3443.
You, H.C., Chang, C.M., Liu, T.F., Cheng, C.C., Chang, F.C., Ko, F. H., 2012. Facile preparation of sol–gel-derived ultrathin and high-dielectric zirconia films for capacitor devices. Appl. Surf. Sci. 258 (24), 10084–10088.
Zeng, J., Guo, J., Sun, Z., Deng, F., Ning, C., Xie, Y., 2020. Osteoblastic and anti-osteoclastic activities of strontium-substituted silicocarnotite ceramics: in vitro and in vivo studies. Bioact. Mater. 5 (3), 435–446.
Zhu, W., Fujiwara, A., Nishiike, N., Nakashima, S., Gu, H., Marin, E., Pezzotti, G., 2018. Mechanisms induced by transition metal contaminants and their effect on the hydrothermal stability of zirconia-containing bioceramics: an XPS study. Phys. Chem. Chem. Phys. 20 (45), 28929–28940.
Zientara, M., Jakubczyk, D., Litniewski, M., Hołyst, R., 2013. Transport of mass at the nanoscale during evaporation of droplets: the Hertz-Knudsen equation at the nanoscale. J. Phys. Chem. C 117 (2), 1146–1150.